Defect detection inside superconducting 1.3 GHz cavities by means of x-ray fluorescence spectroscopy

M. Bertucci, P. Michelato, M. Moretti, A. Navitski, and C. Pagani

Citation: Rev. Sci. Instrum. **87**, 013103 (2016); doi: 10.1063/1.4939611
View online: http://dx.doi.org/10.1063/1.4939611
View Table of Contents: http://aip.scitation.org/toc/rsi/87/1
Published by the American Institute of Physics

REVIEW OF SCIENTIFIC INSTRUMENTS **87**, 013103 (2016)

Defect detection inside superconducting 1.3 GHz cavities by means of x-ray fluorescence spectroscopy

M. Bertucci,[1] P. Michelato,[1] M. Moretti,[1] A. Navitski,[2] and C. Pagani[1,3]
[1]*INFN Milano–LASA, Segrate, MI, Italy*
[2]*DESY, Hamburg, Germany*
[3]*Dipartimento di Fisica, Università degli Studi di Milano, via Celoria 16, Milano, Italy*

(Received 20 October 2015; accepted 15 December 2015; published online 12 January 2016)

X-ray fluorescence probe for detection of foreign material inclusions on the inner surface of superconducting cavities has been developed and tested. The setup detects trace element content such as a few micrograms of impurities responsible for thermal breakdown phenomena limiting the cavity performance. The setup has been customized for the geometry of 1.3 GHz TESLA-type niobium cavities and focuses on the surface of equator area at around 103 mm from the centre axis of the cavities with around 20 mm detection spot. More precise localization of inclusions can be reconstructed by means of angular or lateral displacement of the cavity. Preliminary tests confirmed a very low detection limit for elements laying in the high efficiency spectrum zone (from 5 to 10 keV), and a high angular resolution allowing an accurate localization of defects within the equator surface. © *2016 AIP Publishing LLC.* [http://dx.doi.org/10.1063/1.4939611]

I. INTRODUCTION

Superconducting radio frequency (SRF) niobium cavities are a key component of current and future efficient particle accelerators producing high-energy and high-intensity beams.[1] The SRF cavities are made from high-purity niobium and undergo a complex multi-step production process to achieve high accelerating gradient E_{acc} and unloaded quality factor Q_0. These quantities, together with the manufacturing yield, drive cost and performance factors such as cryogenics, beam energy, and machine length. The European X-ray Free Electron Laser (EXFEL),[2] currently under construction in Hamburg, requires, for example, 800 TESLA-shape nine-cell 1.3 GHz SRF niobium cavities operating at nominal average E_{acc} of 23.6 MV/m with Q_0 of at least 10.[10] The future International Linear Collider (ILC)[3] would require the production of 16 000 such cavities operating at nominal average gradient of 31.5 MV/m with almost the same Q_0 factor. With such a quantity of cavities to be fabricated, an appropriate quality control (QC) and failure reason clarification become very important issues.

The ability to detect performance-limiting defects on the inner surface, which lead to low Q_0 factor, thermal breakdowns (especially at the equator welding seams and the surrounding area), and x-ray radiation (mainly due to sharp geometric defects on the irises),[4–6] provides a tool of QC and failure reason clarification. Detection of failures and defects, especially in early production steps, would significantly reduce repetition of quite expensive cold RF tests and retreatments of the cavities.

Inspection of the inner cavity surface by an optical system is an inexpensive and useful means for surface control and identification of dangerous or suspicious features.[7,8] It does not provide, however, information about material content in the defect region, which is required for sorting out the cavities with foreign inclusions and for the localisation of a contamination source in the production cycle. Preliminary diagnostic is usually performed during the QC of niobium sheets resorting to several non-destructive methods. Among them, the eddy current scanning method[9] has proven to be the most suitable with a very good performance in terms of resolution, speed, and penetration depth. However, in addition to this prominent *a priori* examination, it would be useful to develop another method allowing *a posteriori* evaluation of defects that could have contaminated the niobium surface during the various phases of cavity production starting from the sheets. When possible, the defect could be then removed with a guided repair procedure such mechanical grinding and local etching.

X-ray fluorescence (XRF) analysis is widely used for elemental and chemical analyses, particularly in the investigation of metals. The complicated shape of the SRF cavities and hidden inner surface, as a most critical one, requires, however, development of a special device. This technique, already employed during the Nb-sheet QC,[9] appears to be entitled for development of a diagnostic tool for the detection of trace element inclusions on the cavity surface. Preliminary feasibility test[10] has been performed employing a portable XRF setup. It consists of an X-ray source with 25 kV accelerating voltage, 200 μA beam current, and 5 W beam power and employs molybdenum target-anode with characteristic X-ray energy K_α at 17.4 keV providing a 2.5 mm diameter spot on the sample. A silicon detector with Peltier cell cooling has been used for the X-ray detection. Even resorting to such a low-performance XRF setup, 10 μg of iron, tungsten, and copper grain samples have been easily detected. Furthermore, the grain positions have been correctly reconstructed by means of lateral scanning. These encouraging results have been the first step towards the development of an XRF tool for the inner surface of 1.3 GHz SRF cavities.

II. X-RAY FLUORESCENCE TECHNIQUE

A. Overview

XRF is a non-destructive elemental analysis technique based on the detection of characteristic X-ray radiation emitted from a material that has been excited by a high-energy primary X-ray source. It allows simultaneous acquisition of the whole sample spectrum in a very short time, detecting low concentration values up till a part per million. The fluorescence spectrum lines offer an unequivocal determination of sample elements. The XRF setup consists of an X-ray source for primary excitation of the material to be investigated and a detection unit for energy or wavelength dispersive spectrometry (Fig. 1).

Typical X-ray source is a Coolidge-like tube with hot cathode (electron emitter) and a metal target as an anode. Tube spectrum is given by bremsstrahlung radiation produced by electron-bombardment of the target along with characteristic fluorescence line of the target material. Tube voltage U sets the cut-off energy of continuous spectrum, E_{cutoff}, which must be greater than absorption edge of the anode material (namely, $1s$ orbital binding energy for K lines) in order to generate characteristic lines of the anode material. Nearly, monochromatic radiation can be obtained by means of transmission filters or crystal-monochromators.

The fluorescent radiation can be analysed either by sorting energies of the photons (energy-dispersive analysis) or by separating the wavelength of the radiation (wavelength-dispersive analysis). Spectrometer for the energy-dispersive analysis is smaller, simpler in design, and has fewer engineering parts and so is most suitable for our application.

In the case of energy-dispersive analysis, the fluorescent X-rays emitted by the material of the sample are detected by a solid-state sensor, which produces a "continuous" distribution of pulses with the voltage proportional to the energy of incoming photons. This signal is then processed by a multichannel analyser producing an accumulating digital spectrum used to obtain analytical data. Proportional counters or various solid-state detectors like PIN diodes, silicon-lithium (Si-Li) or germanium-lithium (Ge-Li), and silicon drift detectors (SDDs) are typically used. An incoming X-ray photon ionises a large number of atoms of the detector with the amount of charges being proportional to the energy of the incoming photon. The charges are collected and the spectrum is built up.

Thickness of the active layer of conventional Si-Li detectors can reach up to 5 mm, while maximum thickness for SDD is of the order of 300 μm. This corresponds to higher intrinsic efficiency for standard Si-Li detector comparing to the SDD ones. On the other hand, the advantage of SDD is a very good energy resolution and the capability of a high counting rate of up to more than 10^5 counts/s.

The detectors require cooling, which is normally obtained by liquid nitrogen (77 K), while in the most modern detectors, the use of Peltier cells allows much easier portability and is the best choice for our application.

It must be pointed out that, since the niobium X-ray absorption cross section is high for energies below 100 keV, the excitation radiation will penetrate inside the bulk for a depth of about 68 μm when employing an X-ray tube with the molybdenum anode. The penetration depth corresponds to an inverse of attenuation linear coefficient of niobium μ_{Nb} of 146 cm^{-1} at the energy of Mo K_α line of 17.4 keV.[11] This means that XRF analysis has to be considered as a "surface" analysis technique. Nevertheless, since RF penetration depth in niobium is just around 36 nm,[12] the XRF technique should cover the whole depth of interest.

B. Estimation of the required sensitivity

Presence of small normal-conductive inclusions on the inner cavity surface is one of the main limitations of cavity performance, especially at high gradients. Normal-conducting inclusions dissipate the RF power in the cavity and lead at first to reduction of the quality factor Q_0 of the cavities. Thermal breakdown, or quench, occurs when defect temperature reaches the superconducting critical temperature T_c of niobium; it becomes normal conducting near the defect region and rapidly dissipates all the stored energy in the cavity. The field at which thermal breakdown occurs depends upon many factors such as thermal conductivity of niobium and thereby residual-resistivity ratio (RRR), defect size, and surface resistance of an inclusion. According to a simple model for heat propagation on an inclusion to niobium interface,[13] the quench field can be estimated as

$$H_{max} = \sqrt{\frac{4k(T_c - T_b)}{aR_n}}, \tag{1}$$

where k is the thermal conductivity of niobium, T_c is the superconducting critical temperature of niobium, T_b is the temperature of the helium bath, a is the defect radius, and R_n is the surface resistance of an inclusion.

Quench events are likely to occur near the equators of the cavity-cells, where magnetic field has the highest value, namely, peak surface magnetic field H_{pk}. Assuming a position next to the equator, the defect sees the peak surface magnetic field, which is proportional to the accelerating gradient E_{acc},

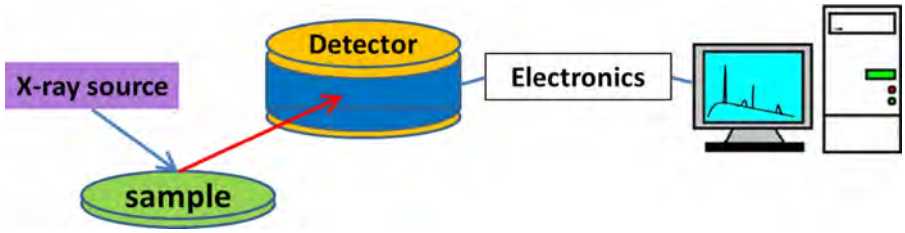

FIG. 1. Schematic overview of the XRF setup.

TABLE I. Critical defect sizes for different materials calculated at different accelerating gradients.

Material	σ (S/m)	R_n (mΩ)	a (μm)		
			15 MV/m	20 MV/m	25 MV/m
ETP Cu (RRR = 50)	$3.8 \times 10^{+9}$	2.0	416	234	150
OF Cu (RRR > 400)	$2.5 \times 10^{+10}$	8.6	1065	600	384
316L SS	$2.1 \times 10^{+8}$	14.7	97	55	35
6061-T6 Al (RRR = 2)	$7.1 \times 10^{+7}$	0.8	57	32	21
Ta—pure	$1.0 \times 10^{+9}$	3.9	213	120	77
Ti—pure	$5.0 \times 10^{+07}$	18	47	27	21
WC	$5.0 \times 10^{+07}$	17.5	47	27	17

so that rearranging Eq. (1), we obtain

$$a = \frac{4k(T_c - T_b)}{R_n\left(\frac{H_p}{E_{acc}}\right)^2 {E_{acc}}^2}. \tag{2}$$

For 1.3 GHz TESLA-shape niobium cavities, typical value of the ratio of peak surface magnetic field to accelerating gradient is 3389 (A/m)/(MV/m). Table I shows some critical defect sizes calculated using Eq. (2) for various materials involved in the cavity production cycle and for different accelerating gradients. Low temperature values of electrical conductivity are extracted from several technical references.[14–17] Electrolytic tough pitch copper (ETP Cu), oxygen-free copper (OF Cu), stainless steel (316L SS), aluminium alloy (6061-T6 Al), pure tantalum (Ta-pure), commercially pure titanium (Ti-pure), and tungsten-carbide (WC) have been used for the analysis. He bath temperature T_b is assumed to be 2 K, and a 75 W/mK average thermal conductivity (corresponding to RRR = 300) is chosen.

Foreign inclusions of a good conductor like copper with a low surface resistance can be tolerated up to a large critical defect-size. Such a big defect can be detected by a direct visual inspection even without magnification. Oxidation or any modifications of the inclusions might increase, however, the surface resistance and finally decrease the critical defect-size. Inclusions of low-conductivity materials have critical defect size in the order of a few tens of micrometer or even less. Therefore, aiming to become an additional method of elemental characterization and identification of foreign inclusions so allowing an incisive control of the inner cavity surface, X-ray fluorescence technique must be in position to have a sensitivity greater than the critical defect size of possible inclusions.

C. Minimum detection limit (mdl)

The relevant number of counts in the XRF spectrum needed for the identification of a given element can be defined by means of the so-called *mdl*,[18] namely, the minimum detectable concentration for the given element (i). According to its most current definition, *mdl* is the concentration corresponding to three times the standard deviation of background intensity I_B in the spectral zone of the chosen X-ray line.[19] If the concentration of element (i) is low, its contribution to exciting and fluorescence radiation absorption can be neglected so that one can assume a linear relation between concentration c_i and XRF line intensity I_i of element (i),

$$I_i \cong I_B + S_i \cdot c_i, \tag{3}$$

where S_i is the sensitivity coefficient for the element (i), which depends on the sample composition and on properties of the experimental setup such as excitation geometry, exciting spectrum, and detector efficiency.

Under this assumption, the minimum detection limit can be calculated as

$$mdl_i = 3\sqrt{I_B}/S_i, \tag{4}$$

where I_B is the background signal intensity in the spectral zone of the element (i). A Poissonian distribution,

$$\sigma_B = \sqrt{I_B}, \tag{5}$$

is assumed in calculating the standard deviation of background intensity.

Aiming to analyse an entirely metallic sample with a nearly monochromatic radiation, we expect to have high sensitivity for medium Z elements (above 25) due to high photoelectric cross section for excitation energy and a low continuous background due to low scattering cross section for residual bremsstrahlung. Benchtop XRF setups easily attain a ppm level minimum detection limit for elements with characteristic K lines lying in the spectrum zone from 5 to 15 keV.[20]

The sensitivity coefficient for each element (i) can be experimentally evaluated by means of Eq. (3), measuring the XRF intensity corresponding to different analyte concentrations. An example of this procedure is reported in Sec. IV.

D. Detection "window"

There are several issues limiting the capability of detection of an XRF system. Beryllium (Z of 4) is the lightest element that can be detected by the XRF, in principle. However, due to low X-ray yield for the light elements and some instrumentation limitations, elements lighter than sodium (Z of 11) are difficult to quantify unless background and very comprehensive inter-element corrections are performed. Fluorescence process is inefficient and the secondary radiation is much weaker than the primary one. The radiation from lighter elements is of relatively low energy and has low penetration power. Furthermore, it is significantly attenuated by passing through air. Because of this, the analyses should be performed in vacuum or X-ray chamber with a helium-sweep can be used

with some loss of low-atomic number intensities. Moreover, for elements with low atomic number, the competitive Auger effect is prevailing on photoemission causing low X-ray emission rates. Use of helium-sweep seems to be a reasonable approach for our application.

For a standard semiconductor detector, the efficiency is the highest in the energy range from 6 to 11 keV. Reduction for low energies is mainly due to the absorption by beryllium window of the detector and by air, whereas for higher energies, it is due to a lower photoelectric absorption cross section in the intrinsic active region of the detector-crystal. Moreover, every element with an absorption edge higher than excitation energy of the tube cannot be ionized and produce X-ray fluorescence. The emission of L lines can be exploited instead of K lines in the case of heavy elements (e.g., gold, lead, and tungsten) since L absorption edge is lower than the K one. However, the corresponding characteristic lines must lay in the high efficiency-range of the detector.

As a consequence of these limitations, a detection window, namely, which elements can be detected independently of their concentration, can be defined for every XRF setup. Almost all elements of the most probable inclusions in the cavities like iron ($K_{\alpha 1}$ at 6.4 keV), copper ($K_{\alpha 1}$ at 8.05 keV), titanium ($K_{\alpha 1}$ at 4.51 keV), tungsten ($L_{\alpha 1}$ at 8.4 keV), and tantalum ($L_{\alpha 1}$ at 8.15 keV) are in the detection window. On the other side, such elements like magnesium ($K_{\alpha 1}$ at 1.25 keV), aluminium ($K_{\alpha 1}$ at 1.49 keV), and silicon ($K_{\alpha 1}$ at 1.74 keV) are difficult to detect.

III. EXPERIMENTAL SETUP

The XRF setup for the detection of foreign inclusions in the SRF cavities has been conceived along the same lines as OBACHT system[8] at DESY for high resolution optical inspection of the cavities. It uses linear drive for longitudinal displacement of the cavities and rotational drive for the camera.

The XRF probe, including X-ray source and detector, is customized to enter within around 70 mm diameter of the iris and aside of the high order mode (HOM) couplers of 1.3 GHz TESLA-shape cavities (Fig. 2). Primary goal is inspection of the equator region of the cavities, which is most affected by the foreign inclusions due to high magnetic field. The excitation and detection setup is customized to focus on the equator surface located at about 103 mm from the cavity axis with an intrinsic spot-size of about 10 mm. More precise localization of the inclusions is foreseen by longitudinal and angular surface scanning.

A. X-ray source

The small size X-ray source XRT-30® from PROTO Manufacturing, Inc., with the diameter of around 30 mm and 125 mm length has been chosen due to the space limitations. This is a fine focus X-ray source employing molybdenum target-anode, operating at up to 30 kV accelerating voltage, 10 mA beam current, and 300 W beam power, and is water cooled.

The choice of molybdenum as the anode material has an advantage of reducing the fluorescence from niobium matrix. Since K_α energy of molybdenum is smaller than absorption edge of 18.9 keV of niobium, the sensitivity in the energy range from 1 to 15 keV can be increased. Aiming to obtain a nearly monochromatic radiation, zircon transmission filter is added to the tube-window. This filter with the absorption edge of 17.99 keV, what is slightly higher than K_α energy of molybdenum, essentially reduces the tube continuous spectrum and suppresses the energies above 17.99 keV. It leads finally to a drastic reduction of the fluorescence spectrum of the niobium matrix at high energies as well as in the low energy zone, where scattering cross section is higher. Finally, it leads to an increase of the peak to background ratio for elements with low atomic numbers.

Size of the thermal spot on the target of the X-ray tube is approximately 0.5×0.5 mm^2. The distance from the target to the exit-window from the X-ray is 15 mm. The window is made of 130 μm thick beryllium and has 6 mm opening. The divergence angle of 22°6′ corresponds to 40 mm diameter spot size on the surface at 100 mm distance. In order to reduce the spot size, three different molybdenum collimators (2.5, 5, and 7 mm diameters, respectively) have been prepared.

B. Detector

SDD from XGLab S.R.L.[22] has been chosen. It offers a good performance even with a very small size. The detector has 25 mm^2 and 450 μm thick active layer, on-chip multilayer collimator for high detection solid angle, and nominal energy resolution of 130 eV at the energy of magnesium K_α-line. The detector is read out by an integrated preamplifier (CUBE®) instead of a standard junction gate field-effect transistor (JFET) obtaining optimal performances in terms of data throughput and stability for the energy resolution. Detection of a low level concentration (less than ppm) in a very fast scanning mode (less than 0.3 s of shaping time) is possible. The detector is equipped with a data acquisition system providing low noise and high acquisition speed. Detector, preamplifier, and Peltier cell for cooling are accommodated in a compact box placed on a metal support (heat sink) and connected to a small size biasing board. The signal buffered by the board is carried through a 15 cm flat cable to a connection board, in its turn transferring the detector signal to an external unit containing the amplifier and the multichannel analyser through a LEMO® coaxial cable. An advantage of this configuration is the possibility of long connection cables from the external unit to the detector-preamplifier block minimizing the volume entering into the cavity.

C. XRF probe design

X-ray tube and detecting unit are combined into a single measuring head (Fig. 3) focusing onto a surface at around 100 mm distance with around 30° tilted detector.

The X-ray tube support is made out of polyether ether ketone (PEEK), a colourless organic thermoplastic polymer, which is very resistant to thermal degradation and with good thermal conductivity. The detector heat sink is connected to the

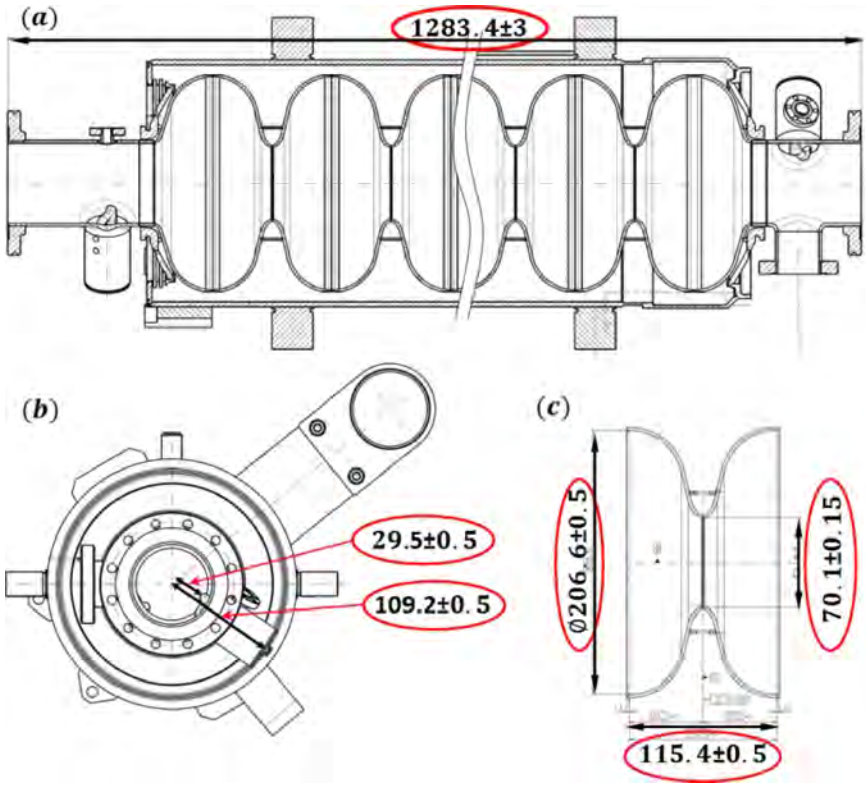

FIG. 2. CAD drawings of 1.3 GHz cavity in the helium tank showing the most important dimensions for the XRF setup, data extracted from Ref. 21.

support by means of a metal slab that can be displaced along the excitation direction. The detector crystal itself is screened from spurious x-ray signals by means of a Mo cylindrical shelter, while a plastic tap protects the detector Be window from accidental impacts. The support also hosts the detector connection board.

A Mo collimator is mounted in front of an x-ray tube window. Placed beside the collimator, a mini-camera allows checking the correct focusing of tube-detector system within the inner cavity volume. A picture of the experimental setup together with a 9-cell 1.3 GHz SRF niobium cavity is shown in Fig. 4.

IV. EXPERIMENTAL RESULTS

A. Definition of parameters of the setup

Tube current, voltage, and filter thickness must be optimized so to achieve a good peak to background ratio, high sensitivity, and appropriate acquisition speed.

Tube voltage governs the energy distribution of the spectrum arriving to the sample. Photoelectric cross section is maximal for excitation energies next to element absorption edge. Since the bremsstrahlung intensity is maximal at a half of the excitation energy, voltage must be, therefore, set to twice of the highest absorption edge energy to be detected.

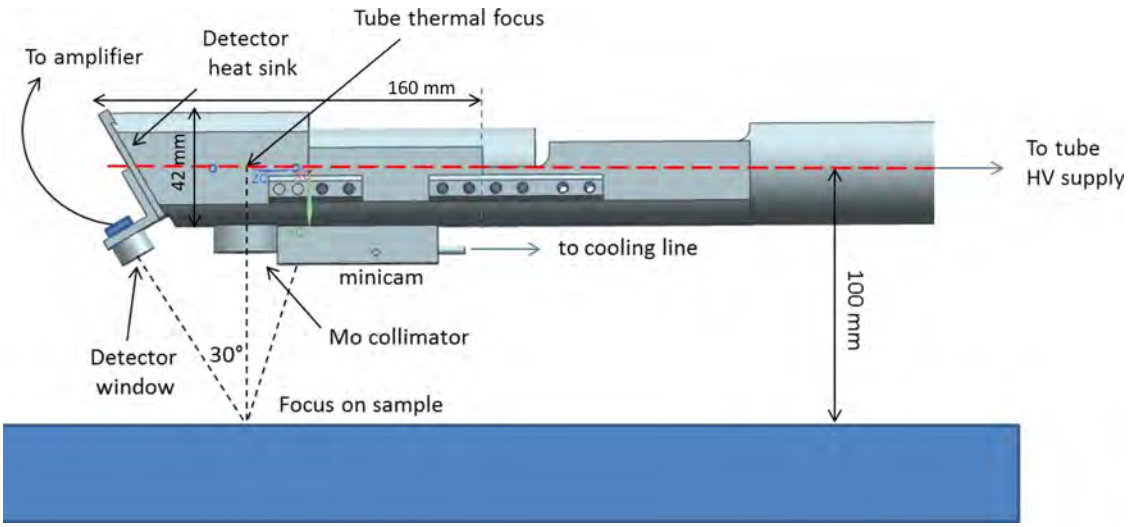

FIG. 3. Schematic sketch of the XRF setup.

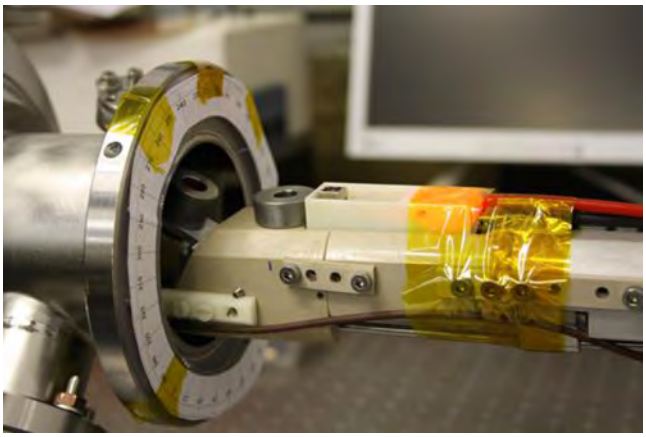

FIG. 4. Picture of XRF probe while entering inside a 9-cell 1.3 GHz SRF niobium cavity.

Moreover, a very intense monochromatic radiation can be obtained only working with a voltage prominently greater than the absorption edge of the anode material. Depending on sample composition, it may be more convenient to exploit the continuous spectrum (higher sensitivity) or the anode primary excitation spectrum (higher count rate).

Tube current essentially controls the net excitation flux rate. This must be enough to minimize the acquisition time but not so high to saturate the detector, whose maximum count rate is $5 \cdot 10^5$ cps for energy resolution below 140 eV. However, the net photon flux on detector is also influenced by tube collimation and attenuation due to the filtering. As already pointed out, the employment of a transmission zirconium filter allows reduction of the background in the spectrum zone with low sensitivity. The importance of filtering is well demonstrated in Fig. 5. A niobium sheet-sample is analysed with and without filtering. Tube settings in this case are 20 kV accelerating voltage and 5 mA current. Together with the characteristic fluorescence spectrum, niobium diffraction lines are clearly visible in Fig. 5(a). The structure of niobium usually used for cavities is polycrystalline (body centred cubic (BCC) structure with lattice parameter a of 0.3294 nm). This means that the whole diffraction pattern is simultaneously excited by the energy values observing the Bragg condition,

$$\lambda = \frac{hc}{E} = 2d_{[hkl]} \sin\theta, \tag{6}$$

$$d_{[hkl]} = d/\sqrt{h^2 + k^2 + l^2}, \tag{7}$$

where θ is the scattering angle (single crystal-exciting radiation) and is the lattice spacing corresponding to the crystal planes identified by Miller indexes $[h, k, l]$.

The diffraction spectrum overlaps with the XRF spectrum and could prevent a correct identification of low-concentration elements. The suppression of tube continuous radiation by means of a transmission filter is, therefore, essential. Fig 5(b) shows the effect of 0.25 mm thick zirconium sheet placed in front of the collimator to suppress the bremsstrahlung radiation of the tube. The diffraction pattern vanishes in the low energy zone, whereas the X-ray fluorescence characteristic lines are still excited by the radiation in the "passband" of the zirconium filter. As an example, the K_α peak of nickel (E of 7.46 keV) is now clearly visible. This is an example of surface

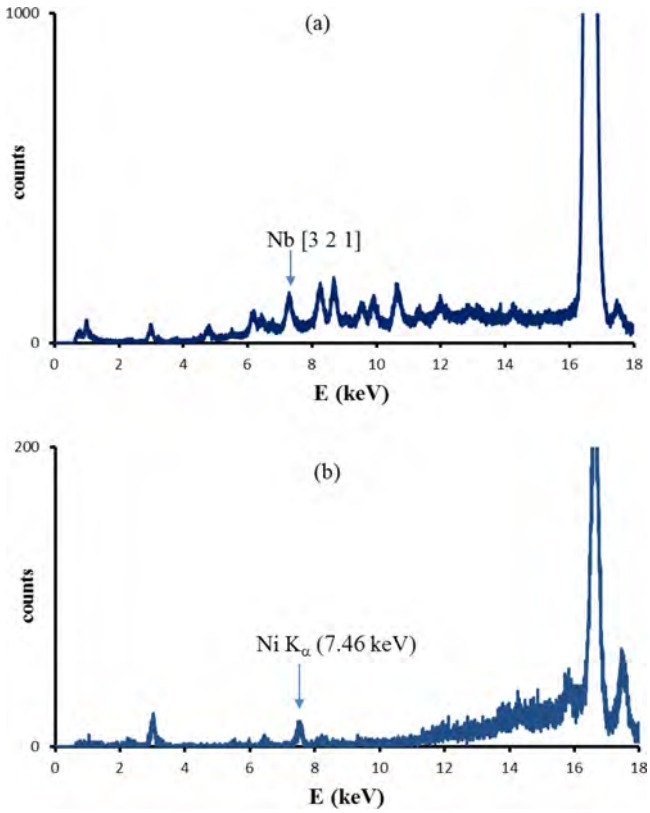

FIG. 5. XRF spectra of a niobium sample acquired without (a) and with (b) a zirconium transmission filter. An effect of the filtering is clearly visible in the energy range from 4 to 10 keV.

contamination, in this case probably due to sample handling that can be disclosed only resorting to a proper spectrum filtering. At any rate, an excessive spectrum filtering may, however, critically attenuate the excitation radiation and drastically reduce the acquisition speed.

Fig. 6 shows a spectrum of a niobium sheet-sample obtained with 0.125 thick zirconium filter and setting the tube voltage to 25 kV. Some diffraction peak survives due to the incomplete continuous spectrum attenuation for energies above 10 keV. On the other hand, it is possible to clearly detect the fluorescence signal of tantalum, which is a metal

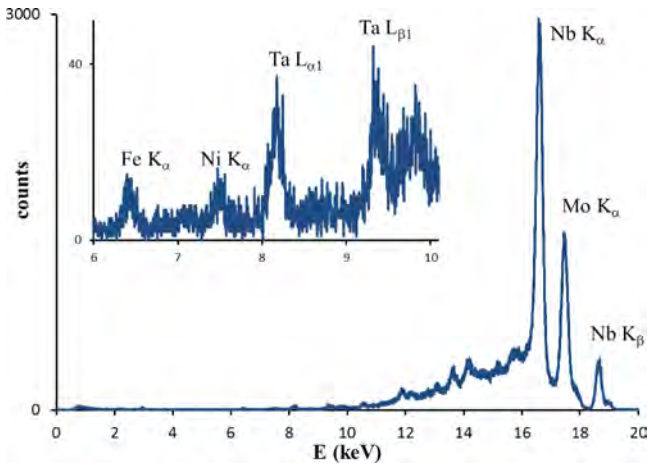

FIG. 6. XRF spectrum of a niobium sample with a magnified view in the range from 6 to 10 keV (inset).

TABLE II. Critical size, mass, and concentration for several materials at E_{acc} of 20 MV/m.

Material	Critical size (μm)	Mass (μg)	Concentration (ppm)
ETP Cu (RRR = 50)	234	240	1810
OF Cu (RRR > 400)	599	4040	11900
316L SS	54.7	2.69	86.9
6061-T6 Al (RRR = 2)	32	0.185	10.2
Ta—pure	120	59.9	881
Ti—pure	26.1	0.169	11.4
WC	26.8	0.630	41.5

impurity usually present in niobium with concentrations below 500 ppm.[23] Additionally, *L* lines of tantalum and *K* lines of iron and nickel are visible. These elements are present in niobium composition with concentrations below few tens of ppm. Despite a proper cleaning, the signal could be also due to a surface contamination.

B. Setup detection limit

Table II shows the critical defect size of most probable surface contaminations at 20 MV/m. The corresponding masses and the expected mass concentrations are calculated assuming 1 cm^2 irradiated spot on niobium sample. A hemispherical defect is assumed for the mass calculation following the same model previously exploited for the quench field calculation.[13] For effective defect detection, the minimum detection limits must be at least comparable to the critical mass concentration.

In order to evaluate the *mdl*, the sensitivity coefficient must be experimentally calculated resorting to Eq. (3). For this, several samples with micrometer-size grains of the same analyte have been prepared. Grain surface *S* has been measured by means of an optical microscope, and their thickness *d* is assumed as the one actually seen by the x-ray radiation (namely, the minimum between penetration depth and escape depth), so that a rough assessment of defect mass is obtained as the product of concentration, grain surface, and thickness.

The grains are dropped on the same niobium surface, so to simulate the experimental conditions as during the analysis of the inner cavity-surface. The fluorescence spectrum is acquired and the characteristic line intensity is plotted as a function of grain mass. Background radiation I_B and sensitivity coefficient S_i are then obtained by means of linear extrapolation. As an example, Fig. 7 shows the calibration line obtained for titanium.

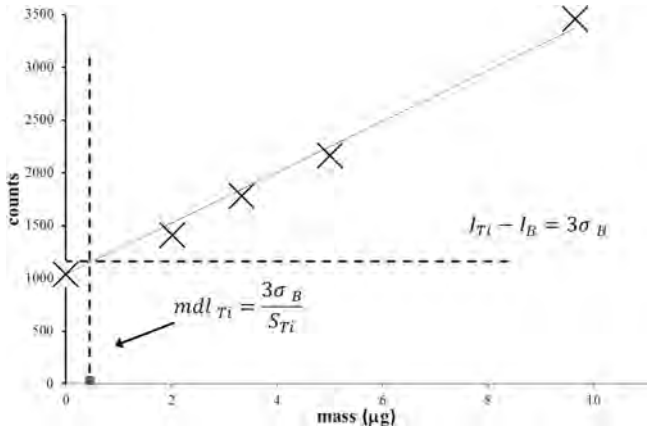

FIG. 7. Intensity of K_α line of titanium (4.5 keV) as a function of grain mass. Vertical and horizontal dotted lines identify the calculated *mdl* and its corresponding fluorescence intensity.

In this case, the sensitivity factor S_{Ti} of 254 counts/μg has been obtained for titanium. It corresponds to the minimum detection limit of 0.36 μg and the minimum detection size of 33.8 μm. This value is of the same order of magnitude as critical mass of titanium reported in Table II. Evaluating the critical field for a 33.8 μm size titanium particle with Eq. (1), one can conclude that the XRF probe is able to detect titanium defects as small as the one responsible for thermal breakdown at fields below 20 MV/m.

Table III summarizes the results of sensitivity coefficient and detection limit measurement for all the materials considered. One can state at this point that the XRF instrument is able to detect defects with masses below the critical values for thermal breakdown in all the cases except for aluminium, whose sensitivity coefficient is significantly low compared to the others. A poor XRF performance with Al was expected under the circumstances outlined in Section II D.

C. Setup scanning resolution

Aiming to assess the setup capability to detect very low element concentrations, several tests have been performed dropping micrometre-size metallic grains on a niobium flat surface. The niobium sample is placed on a precision linear actuator in order to position the defect within the excitation-detection focus area and to perform a lateral sample scanning. Fig. 8 shows the XRF spectrum of an iron defect together with the white spectrum (taken on a defect-free zone of the niobium surface). Tube settings are 25 kV accelerating voltage, 5 mA current, and 60 s acquisition time. The K_α peak of iron at

TABLE III. Minimum detection limits for several materials of interest.

Material	Sensitivity coefficient (counts/μg)	*mdl* (μg)	*mdl* (ppm)	Size at *mdl* (μm)
ETP Cu (RRR = 50)	1063	0.13	12	19
OF Cu (RRR > 400)	1063	0.13	12	19
316L SS	692	0.35	22	28
6061-T6 Al (RRR = 2)	0.04	3900	7800	884
Ta—pure	516	0.26	23	20
Ti—pure	254	0.36	19	34
WC	1012	0.09	11	14

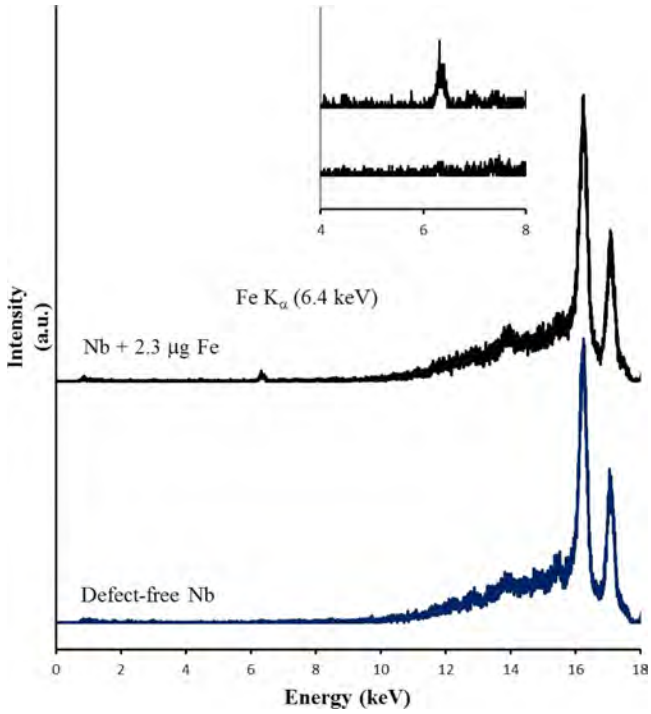

FIG. 8. XRF spectrum of a niobium sample with and without around 2.3 μg iron impurity. The magnified view shows the spectrum in the range from 4 to 8 keV (inset).

6.4 keV is clearly visible. Defect mass is estimated to be around 2.3 μg applying additionally an optical microscope.

Fig. 9 shows the peak intensity variation as a function of defect lateral displacement. The sudden rise in peak intensity occurs when crossing the "dark"/"half-light"/"light" zones. Position 0 corresponds to the true position of the defect. The single step corresponds to 0.5 mm shift. The true defect position can be, therefore, easily reconstructed as the average point between the two drops of peak intensity or by fitting the curve with the Gaussian function and tacking the maximum of it.

As a final step for assessing the setup performance for the specific task, we reproduced step-by-step the experimental conditions at which the XRF setup will be employed. Fig. 10 shows a schematic view of this experimental system.

A single 1.3 GHz niobium cell is settled on a rotating support driven by a direct current (DC) rotary motor, coupled

FIG. 9. Line intensity of K_α peak of iron as a function of lateral displacement of the sample with 0.5 mm steps. Step 0 corresponds to the true defect-position.

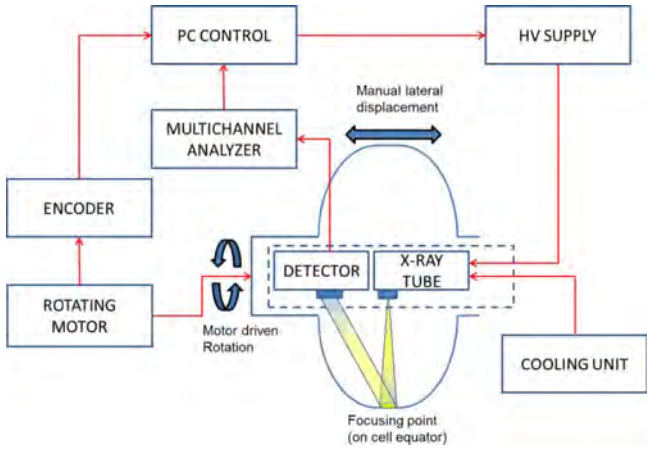

FIG. 10. Schematic view of the experimental setup for XRF scanning of 1.3 GHz niobium cavities with angular and lateral displacements.

with an absolute 1000 pulses per revolution (ppr) encoder allowing the measurement of angular cell displacement from a reference position. The correct focusing of the XRF probe on the equator can be achieved by a manual displacement of the cell-support. A computer (PC) unit remotely controls the power supply of the X-ray tube and acquires the XRF spectra with a customised multichannel acquisition (MCA) readout software. Setup-cooling is achieved by operating at 20 °C.

The defects are simulated by placing metallic particles of different sizes on the cell equator (in the welding zone) at given angular positions. The goal was to obtain the predicted particle position employing the XRF probe as an angular mapping tool.

The results for a 3 μg copper particle are shown in Fig. 11, where the intensity of K_α peak (8.047 keV) of copper is plotted as a function of the angular position.

Two different collimators with 3 and 7 mm diameter have been employed, corresponding to 9 and 20 mm size of the beam spot on the sample surface. The mean value between the edges of the central plateau can be taken as a good assessment of the defect position. The results indicate the accuracy of the defects' localization of a few degrees, what is enough for the

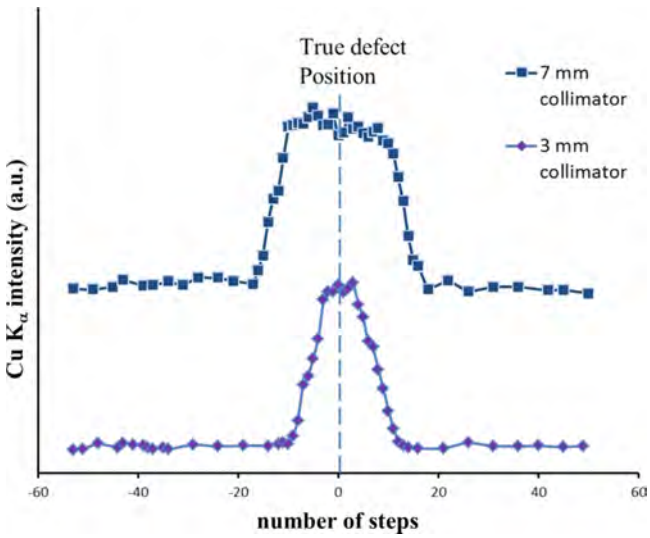

FIG. 11. Intensity of K_α peak (8.047 keV) of copper as a function of angular displacement. Two different collimators of 3 and 7 mm have been used.

application of further surface mapping and repair techniques like optical inspection and local grinding.

V. CONCLUSIONS

New diagnostic probe based on X-ray fluorescence spectroscopy for inspection of SRF cavities has been designed, developed, and tested. It allows detection of foreign material inclusions on the inner surface of the cavities. The results so far obtained put into light the good performances of the setup with the minimum detection limit as low as few microgram for metallic impurities with characteristic X-ray lines laying in the high efficiency spectrum zone from 5 to 10 keV. The XRF instrument is able to detect the most probably defects with masses below the critical values for thermal breakdown except for aluminium, whose sensitivity coefficient is significantly low compared to the others. Moreover, with a proper modification of excitation-detection focusing geometry, the same apparatus could be used for detecting foreign contamination at the iris locations inducing enhanced field emission, which is another one of the main limitations to high gradient cavity performances.[24]

An accurate localization of defects on the surface has been demonstrated by the angular and lateral displacements of the cavity too. This preliminary trial stage of the setup can be considered concluded with a full achievement of the expected performances, so enabling a new analytic tool that will extend the outreach for diagnostics of cavity-defects.

[1]H. Padamsee, J. Knobloch, and T. Hays, *RF Superconductivity for Accelerators* (Wiley-VCH, New York, 2008), pp. 3–36.
[2]The European x-ray free-electron laser, Technical Design Report No. DESY 2006-097, 2007, http://xfel.eu/en/documents.
[3]ILC Technical Design Report, June 2013, www.linearcollider.org.
[4]H. Padamsee, *RF Superconductivity* (Wiley-VCH, 2008).
[5]A. Navitski, *Scanning Field Emission Microscopy: Scanning Field Emission Investigations of Structured CNT and MNW Cathodes, Niobium Surfaces and Photocathodes* (Südwestdeutscher Verlag für Hochschulschrifte, 2011), ISBN-13: 978-3838124896.
[6]A. Navitski, S. Lagotzky, D. Reschke, X. Singer, and G. Müller, "Field emitter activation on cleaned crystalline niobium surfaces relevant for superconducting rf technology," Phys. Rev. Spec. Top.–Accel. Beams **16**, 112001 (2013).
[7]T. Harden, M. Borden, A. Canabal, P. Pittman, and T. Tajima, "Preconceptual design of automated systems for SRF cavity assembly and optical inspection," in *Proceedings of PAC07*, *Albuquerque, New Mexico WEPMS032* (2007).
[8]Y. Iwashita, Y. Tajima, and H. Hayano, Phys. Rev. Spec. Top.–Accel. Beams **11**, 093501 (2008).
[9]W. Singer, D. Proach, and A. Brinkmann, in *Proceedings of the 1997 Workshop on RF Superconductivity*, *Abano Terme, Padova, Italy*, *October 6-10 1997*, edited by V. Palmieri and A. Lombardi (Istituto Nazionale di Fisica Nucleare, Società Italiana di Fisica, Università degli Studi di Pavia, 1998), p. 850.
[10]P. Michelato, M. Bertucci, A. Navitski, W. Singer, X. Singer, C. Pagani, and Y. Tamashevich, in *Proceedings of the 16th International Conference on RF Superconductivity*, *Paris, France*, *September 23-27 2013*, edited by C. Antoine, S. Bousson, and G. Martinet (Institut de Physique Nucléaire Orsay, 2014), pp. 736–739.
[11]National Institute of Standards and Technology, Physical Measurement Laboratory, http://physics.nist.gov.
[12]N. W. Ashcroft and N. D. Mermin, *Solid State Physics* (Harcourt, 1976), pp. 737–739.
[13]H. Padamsee, J. Knobloch, and T. Hays, *RF Superconductivity for Accelerators* (Wiley-VCH, New York, 2008), pp. 205–206.
[14]P. D. Desai, T. K. Chu, H. M. James, and C. Y. Ho, J. Phys. Chem. Ref. Data **13**(4), 1069 (1984).
[15]Institute for Cryomaterials, Handbook of Materials for Superconducting Machinery (Battelle Columbus Labs, 1977), sec. 10.1.4.
[16]M. V. Handsen and W. S. Williams, J. Am. Ceram. Soc. **74**(6), 1411 (1991).
[17]E. W. Klinard and C. P. Kempter, J. Less-Common Met. **15**, 59 (1968).
[18]R. Jenkins and J. V. Gilfrich, X-Ray Spectrom. **21**, 263 (1992).
[19]D. MacDougall, W. Crummett *et al.*, Anal. Chem. **52**, 2242–2249 (1980).
[20]R. O. Miller, *Spectrochemical Analysis by X-ray Fluorescence* (Plenum Press, New York, 1972), pp. 128–132.
[21]Specification Documents for Production of European XFEL 1.3 GHz SC Cavities, DESY, not public, 2009.
[22]L. Bombelli, C. Fiorini, T. Frizzi, R. Alberti, and R. Quaglia, in *Proceedings of NSS/MIC 2012*, *Anaheim, CA, USA*, *October 27-November 3 2012* (IEEE, 2012), pp. 418–420.
[23]W. Singer and D. Proch, in *Proceedings of the XV Conference on Charged Particles Accelerators*, *Protvino, Russia*, *October 22-24 1996*, edited by A. A. Aseev (IHEP, 1996), pp. 127–135.
[24]Y. Li, K. Liu, R. Geng, and A. Palczewski, in *Proceedings of the 16th International Conference on RF Superconductivity*, *Paris, France*, *September 23-27 2013*, edited by C. Antoine, S. Bousson, and G. Martinet (Institut de Physique Nucléaire Orsay, 2014), pp. 392–397.